CMS Physics Analysis Summary

Contact: cms-pag-conveners-b2g@cern.ch 2017/12/12

Search for third-generation scalar leptoquarks decaying to a top quark and a τ lepton at $\sqrt{s} = 13$ TeV

The CMS Collaboration

Abstract

A search for pair production of heavy scalar leptoquarks (LQs) decaying into a top quark and a τ lepton is presented. The search considers final states with an electron or a muon, one or two τ leptons decaying to hadrons, and additional jets. The data collected in proton-proton collisions in 2016 at $\sqrt{s} = 13$ TeV with the CMS detector at the LHC, corresponding to an integrated luminosity of 35.9 fb^{-1} are used. No evidence for pair production of leptoquarks is found. Upper limits on the production cross section are set as a function of LQ mass, assuming a branching fraction of unity for the decay LQ $\rightarrow$ tτ, excluding masses below 900 GeV at 95% confidence level. These results provide the most stringent exclusion limits on the production of scalar leptoquarks in the top quark and τ lepton decay channel to date.

1 Introduction

Leptoquarks (LQs) are hypothetical particles that carry both baryon and lepton quantum numbers. They are charged under all standard model (SM) gauge groups and their possible quantum numbers can be restricted by the assumption that their interactions with SM fermions are renormalizable and gauge invariant [1]. The spin of an LQ state is either 0 (scalar LQ) or 1 (vector LQ). Leptoquarks appear in theories beyond the standard model such as grand unified theories [2–4], technicolor models [5, 6], or compositeness scenarios [7, 8].

Third-generation scalar LQs have recently received considerable theoretical interest, as they can explain an anomaly in the $\bar{B} \to D\tau\bar{\nu}$ and $\bar{B} \to D^*\tau\bar{\nu}$ decay rates reported by the BaBar [9, 10], Belle [11–13], and LHCb [14] Collaborations, which deviate from the SM predictions by about four standard deviations [15]. Studies of the flavor structure of LQ couplings revealed that large couplings to third-generation quarks and leptons would explain this anomaly [16–19]. Third-generation LQs can appear in a unified theory in which only third-generation quarks and leptons are unified [20, 21] and therefore their existence is not constrained by proton decay experiments. All of these models, which predict LQs with masses at the TeV scale and sizable couplings to top quarks and τ leptons, can be tested at the CERN LHC.

This paper presents the first search for a third-generation scalar LQ (LQ_3) decaying into a top quark and a τ lepton at a center-of-mass energy $\sqrt{s} = 13\,\text{TeV}$. A previous search for this channel at $\sqrt{s} = 8\,\text{TeV}$ by the CMS Collaboration resulted in a lower mass limit of 685 GeV for a branching fraction $\beta = 1$ into a top quark and a τ lepton [22]. Other searches for an LQ_3 have targeted the decays $LQ_3 \to b\nu$ and $LQ_3 \to b\tau$ [23–31]. The search for LQ_3s presented here can also be interpreted in the context of R-parity [32] violating (RPV) supersymmetric models [33], where the supersymmetric partner of the bottom quark (bottom squark) decays into a top quark and a τ lepton via the RPV coupling.

In proton-proton (pp) collisions LQs are mainly pair produced through the quantum chromodynamic (QCD) quark-antiquark annihilation and gluon-gluon fusion subprocesses. There is also a lepton-mediated $t(u)$-channel contribution that depends on the unknown lepton-quark-LQ Yukawa coupling, but this contribution to LQ_3 production is suppressed at the LHC, as it requires third-generation quarks in the initial state. Hence, the LQ pair production cross section only depends on the assumed values of the LQ spin and mass, and the center-of-mass energy. The corresponding pair production cross sections have been calculated up to next-to-leading order (NLO) in perturbative QCD [34].

We consider events with at least one electron or muon and at least one τ lepton, where the τ lepton undergoes a one- or three-prong hadronic decay, $\tau_h \to \text{hadron(s)} + \nu_\tau$. In $LQ_3\overline{LQ}_3$ decays, τ leptons arise directly from LQ_3 decays, as well as from W bosons in the top quark decay chain. Electrons and muons are produced in leptonic decays of W bosons or τ leptons. Two search regions are used in this analysis: a di-τ region with the signature $\ell\tau_h\tau_h$+X, with high sensitivity for LQ_3 masses below 500 GeV, and one with a single τ lepton in the final state, $\ell\tau_h$+X, which has higher sensitivity for LQ_3 masses above 500 GeV. Here, ℓ denotes either an electron or a muon, and X denotes two or more jets. The dominant backgrounds in this search come from $t\bar{t}$+jets and W+jets production, with jets misidentified as hadronically decaying τ leptons. These backgrounds are estimated through measurements in control regions and extrapolated to the signal region.

In this paper, Section 2 describes the CMS detector, while Section 3 describes the data samples and the properties of simulated events utilized in the analysis. Section 4 outlines the techniques used for object reconstruction and Section 5 describes the selection criteria applied in each

analysis channel. The method used for the background estimation is reported in Section 6, and systematic uncertainties are detailed in Section 7. Finally, Section 8 contains the results of the analysis, and Section 9 summarizes this work.

2 The CMS detector

The central feature of the CMS apparatus [35] is a superconducting solenoid of 6 m internal diameter, providing a magnetic field of 3.8 T. Within the superconducting solenoid volume are a silicon pixel and strip tracker, a lead tungstate crystal electromagnetic calorimeter (ECAL), and a brass and scintillator hadron calorimeter (HCAL). In the region $|\eta| < 1.74$, the HCAL cells have widths of 0.087 in pseudorapidity (η) and 0.087 radians in azimuth (ϕ). In the η–ϕ plane, and for $|\eta| < 1.48$, the HCAL cells map on to 5×5 arrays of ECAL crystals to form calorimeter towers projecting radially outwards from close to the nominal interaction point. At larger values of $|\eta|$, the size of the towers increases and the matching ECAL arrays contain fewer crystals. Electron momenta are estimated by combining the energy measurement in the ECAL with the momentum measurement in the tracker. Extensive forward calorimetry complements the coverage provided by the barrel and endcap detectors. Muons are measured in gas-ionization detectors embedded in the steel flux-return yoke outside the solenoid. A more detailed description of the CMS detector, together with a definition of the coordinate system used and the relevant kinematic variables, can be found in Ref. [35].

3 Data sample and simulated events

The search for LQ_3s presented here is based on pp collisions at $\sqrt{s} = 13$ TeV recorded with the CMS detector in 2016. The data sample corresponds to an integrated luminosity of 35.9 fb^{-1} [36].

The leading order Monte Carlo (MC) program PYTHIA 8.205 [37] is used to simulate the LQ_3 pair production signal process. Both LQs are required to decay into a top quark and a τ lepton. The signal samples are generated for LQ masses ranging from 200 to 2000 GeV.

Background processes for top quark pair production ($t\bar{t}$) via the strong interaction as well as electroweak single top quark production in the t-channel and tW processes are simulated with the NLO generator POWHEG (v1 is used for the single top tW processes and v2 for the single top t-channel and $t\bar{t}$ processes) [38–43]. The s-channel process of single top quark production is generated at NLO using the program MADGRAPH5_AMC@NLO (v2.2.2) [44].Further background processes involve W and Z boson production in association with jet radiation. These processes are generated with MADGRAPH5_AMC@NLO (v2.2.2), W boson production at NLO and Z boson production at LO level. The matrix element generation of W and Z boson production is matched to the parton shower emissions with the FxFx [45] and MLM [46] algorithms, respectively. Background processes from QCD multijet production are simulated with PYTHIA 8.205. For all generated events, PYTHIA 8.205 is used for the description of the parton shower and hadronization. In the parton shower, the underlying event tune CUETP8M1 [47, 48] has been applied for all samples except $t\bar{t}$ and single top quark production in the t-channel that use the underlying event tune CUETP8M2T4 [47, 48]. Furthermore, the event generation is performed using the NNPDF 3.0 parton distribution functions (PDFs) [49] for all events.

4 Event reconstruction

Event reconstruction is based on the CMS particle-flow (PF) algorithm [50], which combines information from all subdetectors, including measurements from the tracking system, energy deposits in the ECAL and HCAL, and tracks reconstructed in the muon detectors. Based on this information, all particles in the event are reconstructed as electrons, muons, photons, charged hadrons, or neutral hadrons.

Primary vertices are reconstructed using a deterministic annealing filtering algorithm [51]. The reconstructed vertex with the largest value of summed p_T squared of the associated track-level physics objects is taken to be the primary interaction vertex. The physics objects are the jets, clustered using the jet finding algorithm [52, 53] applied to all charged tracks associated with the vertex, plus the corresponding associated missing transverse momentum. Charged particles associated with other primary vertices are removed from further consideration.

Muons are reconstructed using the information collected in the muon detectors and the inner tracking detectors, and are measured in the range $|\eta| < 2.4$. Tracks associated with muon candidates must be consistent with a muon originating from the leading primary vertex, and are required to satisfy a set of identification (ID) requirements. Matching muon detector information to tracks measured in the silicon tracker results in a p_T resolution for muons with $20 < p_T < 100\,\text{GeV}$ of 1.3–2.0% in the barrel and less than 6% in the endcaps. The p_T resolution in the barrel is less than 10% for muons with p_T up to 1 TeV [54].

Electron candidates are reconstructed in the range $|\eta| < 2.5$ by combining tracking information with energy deposits in the ECAL. Candidates are identified [55] using information on the spatial distribution of the shower, the track quality, and the spatial match between the track and electromagnetic cluster, the fraction of total cluster energy in the HCAL, and the level of activity in the surrounding tracker and calorimeter regions. The transverse momentum resolution for electrons with $p_T \approx 45\,\text{GeV}$ from $Z \to ee$ decays ranges from 1.7% for nonshowering electrons in the barrel region to 4.5% for electrons showering in the endcaps [55].

Jets are clustered using PF candidates as inputs to the anti-k_T algorithm [52] in the FastJet 3.0 software package [53] using a distance parameter of 0.4. For all jets, corrections based on the jet area [56] are applied to the energy of the jets to remove the energy contributions from neutral hadrons from additional pp interactions in the same or adjacent bunch crossings (pileup collisions). Subsequent corrections are used to account for the nonlinear calorimetric response in both jet energy and mass, as a function of η and p_T [57]. The jet energy resolution amounts typically to 15% at 10 GeV, 8% at 100 GeV, and 4% at 1 TeV [58]. Jets associated with b quarks are identified using the combined secondary vertex v2 (CSVv2) algorithm [59, 60]. The working point used for jet b tagging in this analysis has an efficiency of $\approx$ 65% (in $\bar{t}t$ simulated events) and a mistag rate (the rate at which light-flavor jets are incorrectly tagged) of approximately 1% [60].

Hadronically decaying τ leptons are reconstructed with the hadron-plus-strips (HPS) algorithm [61] and are denoted by τ_h. The HPS algorithm is based on PF jets and combines photons originating from neutral pion decays, reconstructed from the "strips" of ECAL towers, with one or three charged tracks to reconstruct various hadronic decay modes of τ leptons. The cut-based isolation discriminators as described in [62] are used to identify hadronic τ lepton decays.

The missing momentum in the plane transverse to the beam direction is reconstructed as the negative vector sum of the p_T of all PF candidates in the event [63]. Its magnitude is denoted by p_T^{miss}. Corrections to the jet energy scale and jet energy resolution are propagated to the

Table 1: Summary of selection criteria in event categories A (ℓ + τ_h + jets) and B (ℓ + 2τ_h + jets). In category A, two subcategories are defined by the charge of the $\ell\tau_h$ pair.

	Category A		Category B
Lepton selection	opposite-sign $\ell\tau_h$	same-sign $\ell\tau_h$	$\ell\tau_h\tau_h$
Jet selection	at least four jets	at least three jets	at least three jets
p_T^{miss} selection	$p_T^{miss} > 100\,GeV$	$p_T^{miss} > 50\,GeV$	$p_T^{miss} > 50\,GeV$
τ_h selection	$p_T > 100\,GeV$		$p_T^{\tau 1} > 65\,GeV$, $p_T^{\tau 2} > 35\,GeV$
b tagging	at least one b tag		–
S_T selection	–		$S_T > 350\,GeV$
Fit variable	p_T^t in two S_T bins		number of events

measurement of p_T^{miss} [58].

5 Event selection and categorization

In the online trigger system, events with an isolated muon with $p_T > 24\,GeV$ and $|\eta| < 2.4$ are selected in the muon channel. The trigger selection employed in the electron channel requires an electron with $p_T > 27\,GeV$ and $|\eta| < 2.1$. We select events offline containing at least one isolated muon with $p_T > 30\,GeV$ and $|\eta| < 2.4$ or at least one isolated electron with $p_T > 30\,GeV$ and $|\eta| < 2.1$. For the latter, a veto is applied to events with additional muons to avoid overlap between the two channels. At least one τ_h lepton with $p_T > 20\,GeV$ and $|\eta| < 2.1$ and at least two jets with $p_T > 50\,GeV$ and $|\eta| < 2.4$ are required. Events are selected if a third jet with $p_T > 30\,GeV$ and $|\eta| < 2.4$ is present, and any additional jets are only considered if they have $p_T > 30\,GeV$. The p_T^{miss} is required to be above 50 GeV. The events are further divided into two categories to enhance the sensitivity over a broad range of LQ masses. The event selection was chosen to maximize the expected significance of a possible leptoquark signal. A summary of the selection criteria for both categories is given in Table 1 and described below.

5.1 Category A: ℓ + τ_h + jets

In this category, exactly one τ_h lepton is required. Additionally, high transverse momentum requirements are applied to maximize the sensitivity at high LQ masses.

The leading jet is required to have $p_T > 150\,GeV$. In addition we define two subcategories based on the electric charges of the particles in the $\ell\tau_h$ pair: opposite-sign (OS) and same-sign (SS). If the event contains more than one electron or muon, the $\ell\tau_h$ pair with the largest scalar p_T sum is chosen. For both subcategories, we require that the leading tau lepton has $p_T > 100\,GeV$ and that there is at least one b-tagged jet. Events passing the OS $\ell\tau_h$ pair requirement must contain at least four jets and have $p_T^{miss} > 100\,GeV$. Finally the events are divided into two regions of S_T, where S_T is the scalar sum of the p_T of all selected jets, leptons, and p_T^{miss}. In the low-S_T search region events must satisfy $S_T < 1200\,GeV$, and in the high-S_T search region events are required to have $S_T \geq 1200\,GeV$.

The top quarks originating from the decay of a heavy LQ_3 are expected to be produced with larger p_T than the top quarks produced in background processes. Therefore, the transverse momentum distribution of the top quark candidate decaying into hadronic jets (p_T^t) gives discrimination power between background and signal events and the analysis in category A is carried out through a measurement of the p_T^t spectrum.

A kinematic reconstruction of the top quark candidate is performed by building top quark hypotheses using all final-state jets. Each top quark hypothesis is allowed to consider between

one and five jets. Because of the presence of multiple hypotheses in each event, we choose the hypothesis in which the reconstructed top quark mass is closest to the value of 172.5 GeV.

In this category a template-based statistical evaluation using the reconstructed p_T^t is performed.

5.2 Category B: ℓ + 2 τ_h + jets

In this category events are required to have at least two τ_h leptons. This requirement removes a large fraction of the SM background processes as these are usually only selected because they contain other objects misidentified as one or more τ_h leptons. The exception to this are diboson production events which may contain one or more τ_h leptons but the cross sections for these processes are small. The selection criteria in this category are adapted to provide good sensitivity for low leptoquark masses.

Each event is required to contain an OS $\tau_h\tau_h$ pair. If the event contains more than one $\tau_h\tau_h$ pair, the OS pair with the largest scalar p_T sum is selected. Moreover, the leading and subleading τ_h must satisfy $p_T > 65$ GeV and $p_T > 35$ GeV, respectively.

In this category a counting experiment is performed, as the number of expected background events is too small to benefit from a shape-based analysis.

6 Background estimation

The background in this analysis consists of events that are selected because of jets misidentified as τ_h leptons and of SM processes with prompt $\ell\tau_h$ pairs.

In the following, events from $t\bar{t}$ and W+jets production that contain at least one misidentified τ_h lepton are obtained from control regions (CRs) separately defined for the two search regions (SRs) A and B. We consider the following contributions: the $t\bar{t}$ background that consists of only misidentified τ_h leptons (or exactly one misidentified τ_h lepton as in category A), denoted by $t\bar{t}_f$, the $t\bar{t}$ background that consists of (at least) one prompt τ_h lepton and (at least) one misidentified τ_h lepton (only used in category B), denoted by $t\bar{t}_{p+f}$, and the $t\bar{t}$ background that consists of one prompt τ_h lepton, denoted by $t\bar{t}_p$.

An extrapolation method is used to derive the background due to misidentified τ_h leptons. The normalization, and in category A also the shape, of the $t\bar{t}$ background is estimated using

$$N_{SR}^{t\bar{t},data} = (N_{CR}^{data} - N_{CR}^{other,MC}) \cdot \frac{N_{SR}^{t\bar{t},MC}}{N_{CR}^{t\bar{t},MC}}, \quad (1)$$

where N is the total number of events for the respective process in the signal region or control region and where other denotes all non-$t\bar{t}$ background processes estimated from simulation. The contribution to the background from events with prompt τ_h leptons only is estimated from simulated events.

6.1 Backgrounds in category A

In each subcategory of category A, the largest fraction of background events originates from $t\bar{t}$ production. The second largest source of background events arises from W+jets production, while minor contributions come from single top quark and Z+jets production.

The $t\bar{t}_f$ background and the W+jets background that contain a misidentified τ_h lepton are derived from a single CR, which is defined through the same selection requirements as for the SR, but with an inverted isolation requirement for the τ_h lepton.

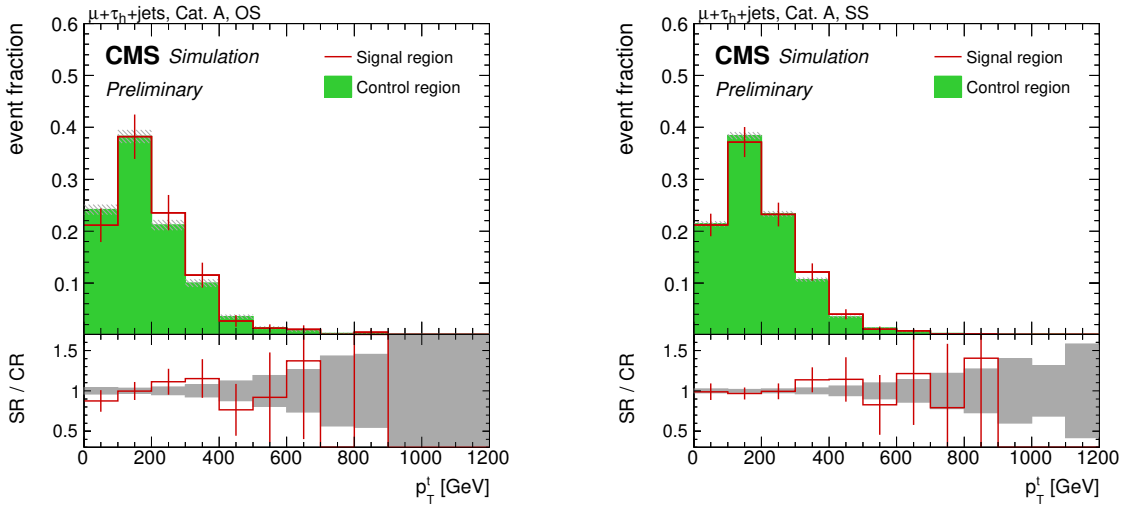

Figure 1: Shape comparison between the signal region A and the corresponding control region, as a function of p_T^t, for simulated $t\bar{t}$ and W+jets events. Events with an opposite-sign $\mu\tau_h$ pair are shown on the left, while those with a same-sign $\mu\tau_h$ pair are shown on the right. The full selection is applied and the S_T categories are combined. All histograms are normalized to the total number of entries. The gray band in the ratio plot corresponds to the statistical uncertainty in the simulated samples.

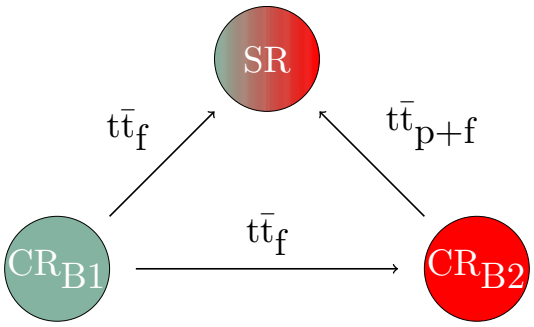

Figure 2: Strategy for the background estimation in category B. The $t\bar{t}_f$ background in the signal region is derived from the control region CR_{B1}. The $t\bar{t}_{p+f}$ background in the signal region is derived from the control region CR_{B2}. To obtain an estimate of the $t\bar{t}_f$ background in the control region CR_{B2}, the control region CR_{B1} is used.

The shape of the p_T^t distribution is compared between the CR and SR in simulated $t\bar{t}$ and W+jets events. Since the inversion of the τ_h isolation criterion introduces kinematic differences between the signal and control regions, a correction is applied in order to reproduce the shape of the $t\bar{t}$ and W+jets background in the SR. After this correction, the shape of the p_T^t distribution for $t\bar{t}$ and W+jets production shows good agreement between the control and signal regions, as shown in Fig. 1.

Once the events in the CR are reweighted, we use Eq. (1) to extrapolate the $t\bar{t}$ and W+jets background yields to the SR. In this equation, we replace $N^{t\bar{t}}$ with $N^{t\bar{t},\,W+jets}$ for category A.

6.2 Backgrounds in category B

In category B, the dominant background originates again from $t\bar{t}$ production. As the fraction of misidentified electrons and muons was found to be negligible in this analysis, at least one of the two τ_h leptons is mimicked by a jet. Thus, events from $t\bar{t}$ production consist either of only

misidentified τ_h leptons or one prompt τ_h lepton and one misidentified τ_h lepton. A separate CR is defined for each component. The strategy for determining this background in category B is shown in Fig. 2.

The first control region (CR_{B1}) is defined by inverting the isolation criterion for all τ_h leptons with respect to the isolation criterion applied in the SR. The region CR_{B1} is used to extrapolate the $t\bar{t}_f$ background to the SR. In contrast to the SR, the charge criterion on the τ_h lepton is removed and the leading τ_h lepton must have $p_T < 100\,\text{GeV}$ to avoid overlap between the control region CR_{B1} and control region CR_A. The $t\bar{t}_f$ background normalization is then derived as in Eq. (1).

A second control region (CR_{B2}) to estimate the $t\bar{t}_{p+f}$ background is defined, in which at least one isolated and at least one nonisolated τ_h lepton are required. In contrast to the SR, the charge criterion on the τ_h lepton is removed and the leading τ_h lepton must have $p_T < 45\,\text{GeV}$. The event must have an opposite-sign $\ell\tau_h$ pair. For this requirement, the pair with the largest summed p_T is chosen. In addition, the events must satisfy $M_T(\ell, p_T^{\text{miss}}) > 100\,\text{GeV}$, where $M_T(\ell, p_T^{\text{miss}})$ is the transverse mass of the lepton-$\vec{p}_T^{\text{miss}}$ system and defined as $M_T(\ell, p_T^{\text{miss}}) = \sqrt{2p_T^{\ell} p_T^{\text{miss}}(1 - \cos(\Delta\phi(\vec{p}_T^{\ell}, \vec{p}_T^{\text{miss}}))}$. The largest non-$t\bar{t}_{p+f}$ fraction in control region CR_{B2} arises from the $t\bar{t}_f$ events. This background is derived from the control region CR_{B1} and extrapolated to the control region CR_{B2} by using the extrapolation method as in Eq. (1). Once the $t\bar{t}_f$ background is estimated from CR_{B1}, it is subtracted from CR_{B2}. The $t\bar{t}_{p+f}$ background is extrapolated to the SR by using the extrapolation method as in Eq. (1).

7 Systematic uncertainties

Systematic uncertainties can affect both the overall normalization of background components, and the shapes of the p_T^t distributions for signal and background processes. Uncertainties in the MC simulation are applied to all simulated events used in the signal and in the various control regions. For each systematic uncertainty, the background estimation procedure described in Section 6 is repeated to study the impact of the respective systematic variation on the final result of the analysis. In the following, the systematic uncertainties applied to the analysis are summarized.

- The uncertainty in the integrated luminosity measurement recorded with the CMS detector in the 2016 run at $\sqrt{s} = 13$ TeV is 2.5% [36].
- We include the following uncertainties in the normalization of the background processes:
  - an uncertainty of 5.6% in the $t\bar{t}$ production cross section [64] for $t\bar{t}$ events that include prompt tau leptons. The contribution to the background from $t\bar{t}$ events that do not contain prompt tau leptons is derived from data.
  - 10% for single top quark [65–67], W+jets, and Z+jets production [68].
  - 20% for diboson production [69, 70].
- The estimation of pileup effects is based on the total inelastic cross section. This cross section is determined to be 69.2 mb. The uncertainty is taken into account by varying the total inelastic cross section by 5% [71].
- Simulated events are corrected for lepton identification, trigger and, isolation efficiencies. The corresponding scale factors are applied as functions of $|\eta|$ and p_T. The systematic uncertainties due to these corrections are taken into account by varying each scale factor within its uncertainty.

Table 2: Summary of largest systematic uncertainties for the $t\bar{t}_f$ (and W+jets) and $t\bar{t}_{p+f}$ backgrounds derived from data, for the $t\bar{t}_p$ background obtained from simulation and for a leptoquark signal with a mass of 700 GeV. Shown is the range of uncertainties within the search regions in category A, and the electron and muon channels.

	Category A			Category B		
Uncertainty	$t\bar{t}_p$	$t\bar{t}_f$ + W+jets	LQ_3	$t\bar{t}_f$	$t\bar{t}_{p+f}$	LQ_3
μ_F, μ_R	26–42%	1–7%	–	5–7%	2–6%	–
τ ID	8–9%	0–1%	9–11%	0%	5–6%	18–20%
BKG estimate	–	6–18%	–	26–30%	30–38%	–

- The scale factors for the jet energy scale (JEC) and the jet energy resolution (JER) are determined as functions of $|\eta|$ and p_T [58]. The effect of the uncertainties in these scale factors are considered by varying the scale factors within their uncertainties. These variations are propagated to the measurement of the missing transverse momentum.
- Scale factors for the b tagging efficiencies are applied. These scale factors are measured as a function of the jet p_T [60]. The corresponding uncertainty is taken into account by varying the scale factors within their uncertainties.
- Various uncertainties in the τ lepton reconstruction are considered. An uncertainty of 5% in the τ lepton identification is applied, with an additional uncertainty of 0.2 $p_T/(1\,\text{TeV})$. An uncertainty of 3% in the τ lepton energy scale is taken into account, and an uncertainty in the charge misidentification rate of 2% is applied [62].
- Parton distribution functions from the NNPDF 3.0 set are used to generate simulated events for both background and signal samples. The uncertainties in the PDFs are determined according to the procedure described in Ref. [72]. The associated PDF uncertainties in the signal acceptance are estimated following the prescription for the LHC [72].
- We consider uncertainties in the renormalization (μ_R) and factorization (μ_F) scales by varying the respective scales (either simultaneously or independently) by factors between 0.5 and 2.
- We apply an uncertainty in the background estimation method by varying the extrapolation factors within their uncertainties. An uncertainty due to the correction factors used to reweight events in control region CR_A is applied.

The systematic uncertainties causing the largest effects on the most important background processes and on the signal are summarized in Table 2. The most important background processes are the $t\bar{t}_f$, $t\bar{t}_f$ and W+jets, and $t\bar{t}_{p+f}$ backgrounds derived from data, and the $t\bar{t}_p$ background taken from simulation. Also shown is an LQ_3 signal with a mass of 700 GeV. The impact of the different sources of uncertainty varies for different processes. The uncertainty due to the scale variation has a large impact on the $t\bar{t}_p$ background, which is taken from simulation. The uncertainty in the τ lepton identification has the largest effect on the signal sample. For the backgrounds derived from several CRs, the uncertainty in the extrapolation factor has the largest impact.

8 Results

The post-fit p_T^t distributions in the electron and muon channels in category A are shown in Figs. 3 and Fig. 4, respectively. Contributions from $t\bar{t}$ and W+jets production with a misidenti-

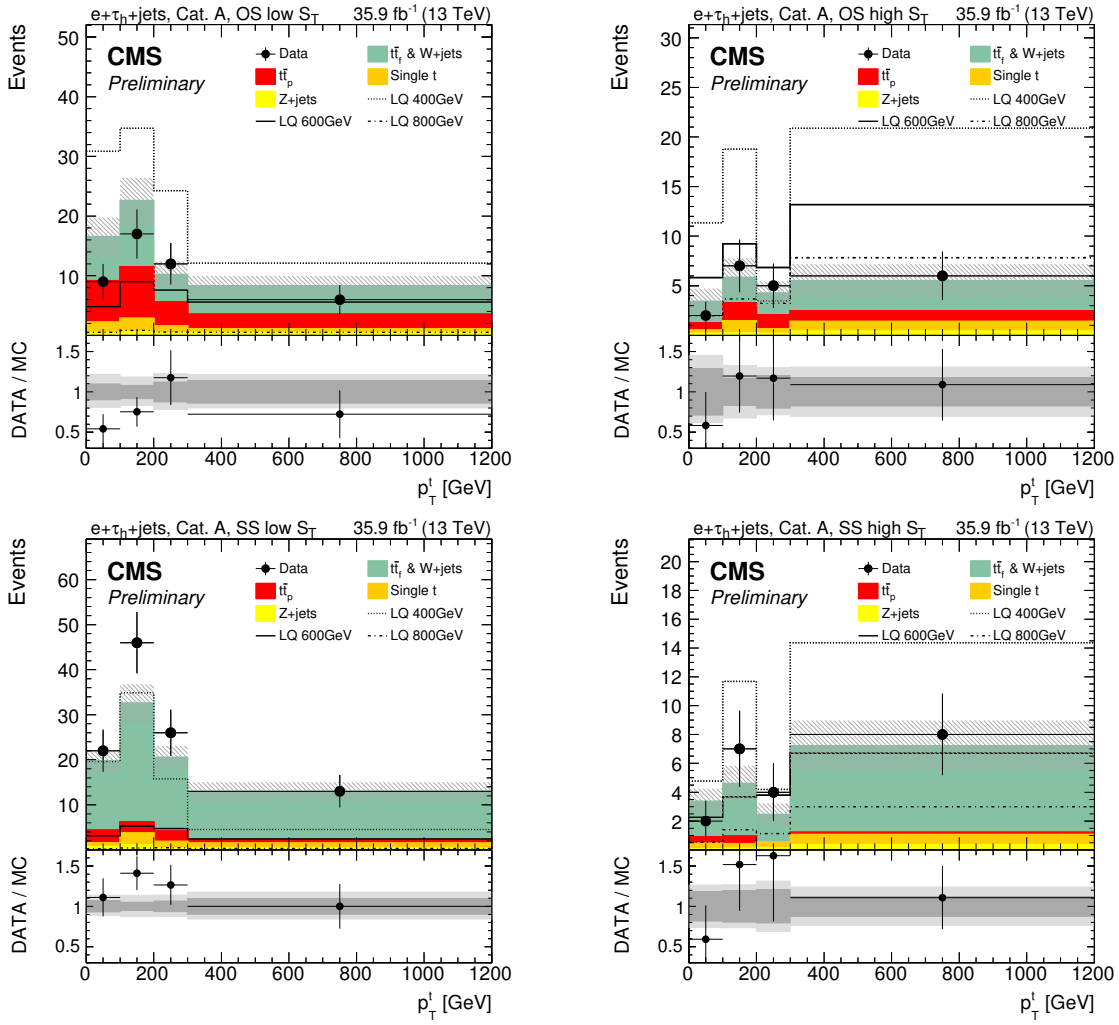

Figure 3: Distributions of p_T^t for events in the electron channel passing the full selection in category A. The events are separated into OS (top), SS (bottom), low S_T (left) and high S_T (right) categories. The hatched areas represent the total uncertainties of the SM background. In the bottom panel, the ratio of data to SM background is shown together with statistical (dark gray) and total (light gray) uncertainties of the total SM background.

fied τ_h lepton are derived from control region CR_A, whereas SM backgrounds with a prompt τ_h lepton and other small backgrounds are taken from simulation.

In Table 3, the total number of events from background processes and signal processes in category B is summarized. No significant deviation from the SM prediction is observed in the data in both categories.

A statistical template-based shape analysis using the measured p_T^t distributions in category A and a counting experiment with the events measured in category B is performed by using the THETA software package [73]. The results of all search categories in the electron and muon channels are combined by using a likelihood fit. Each systematic uncertainty is accounted for by a nuisance parameter in the likelihood formation. For the signal cross section parameter, we use a uniform prior distribution. For the other nuisance parameters, log-normal prior distributions are used. By varying these parameters within their prior distribution functions, pseudo-experiments are performed to estimate the 68 and 95% confidence level (CL) expected limits.

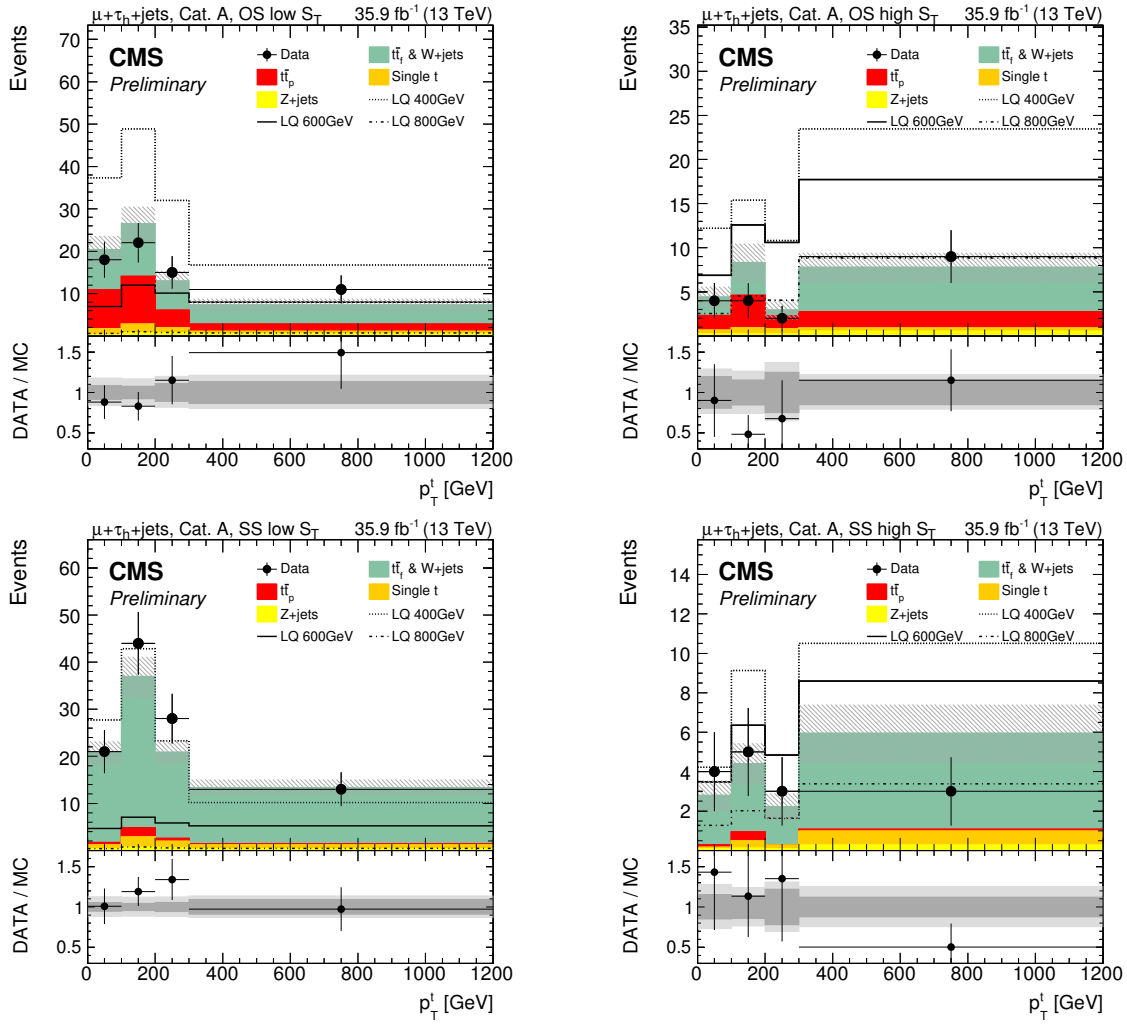

Figure 4: Distributions of $p_{\mathrm{T}}^{\mathrm{t}}$ for events in the muon channel passing the full selection in category A. The events are separated into OS (top), SS (bottom), low S_{T} (left) and high S_{T} (right) categories. The hatched areas represent the total uncertainties of the SM background. In the bottom panel, the ratio of data to SM background is shown together with statistical (dark gray) and total (light gray) uncertainties of the total SM background.

Table 3: Final event yield in category B in the muon and electron channels for different leptoquark mass hypotheses, the background processes and data. The total uncertainties for the signal and the background processes are shown.

Process	$e + \tau_h$ + jets	$\mu + \tau_h$ + jets
LQ_3 (300 GeV)	97^{+25}_{-24}	172^{+38}_{-38}
LQ_3 (400 GeV)	74^{+14}_{-14}	101^{+19}_{-18}
LQ_3 (500 GeV)	$34.6^{+6.7}_{-6.3}$	$46.1^{+8.7}_{-8.1}$
LQ_3 (600 GeV)	$14.3^{+2.9}_{-2.7}$	$22.1^{+4.3}_{-4.0}$
LQ_3 (700 GeV)	$7.5^{+1.6}_{-1.5}$	$7.3^{+1.6}_{-1.5}$
LQ_3 (800 GeV)	$3.3^{+0.7}_{-0.7}$	$4.5^{+1.0}_{-0.9}$
LQ_3 (900 GeV)	$1.6^{+0.4}_{-0.3}$	$1.9^{+0.4}_{-0.4}$
LQ_3 (1000 GeV)	$0.8^{+0.2}_{-0.2}$	$0.9^{+0.2}_{-0.2}$
$t\bar{t}_f$	$2.4^{+0.8}_{-1.1}$	$3.2^{+1.5}_{-1.2}$
$t\bar{t}_{p+f}$	$1.6^{+0.7}_{-0.8}$	$2.1^{+0.8}_{-0.9}$
Single t	$0.3^{+0.3}_{-0.3}$	$0.00^{+0.2}_{-0.0}$
W+jets	$0.5^{+1.2}_{-0.5}$	$0.4^{+0.7}_{-0.4}$
Z+jets	$1.4^{+0.5}_{-0.5}$	$1.0^{+0.4}_{-0.4}$
Diboson	$1.6^{+1.7}_{-1.6}$	$1.7^{+1.8}_{-1.7}$
Total background	$7.8^{+2.4}_{-2.5}$	$8.4^{+2.6}_{-2.4}$
Data	9	11

The 95% CL upper limits on the cross section times β^2 as a function of LQ_3 mass and the 95% CL upper limits on the LQ_3 mass as a function of β are shown in Fig. 5. The cross section for pair production of scalar leptoquarks at NLO accuracy [34] is shown as the dashed line. The dotted lines indicate the uncertainty due to the PDFs and variations of the renormalization and factorization scales by factors of 0.5 and 2.

Production cross sections of 0.6 pb for LQ_3 masses of 300 GeV and about 0.01 pb for masses up to 1.5 TeV are excluded at 95% CL under the assumption of $\beta = 1$ for LQ_3 decays to a top quark and τ lepton. Comparing these limits with the NLO cross section, LQ_3 masses up to 900 GeV (930 GeV expected) can be excluded.

9 Summary

A search has been conducted for pair production of third-generation scalar leptoquarks decaying into a top quark and a τ lepton. The full proton-proton collision dataset recorded in the year 2016 at a center-of-mass energy of 13 TeV, corresponding to an integrated luminosity of 35.9 fb^{-1} has been analyzed. The search has been carried out using the $\ell\tau_h$ and $\ell\tau_h\tau_h$ channels, where SM backgrounds due to misidentified τ_h leptons are derived from control regions. The measured transverse momentum distributions of the reconstructed top quark candidate are analyzed in four search regions in the $\ell\tau_h$ channel. In the $\ell\tau_h\tau_h$ channel the measured number of events is compared to the background prediction and good agreement is found.

Upper limits on the production cross section of leptoquark pairs are set between 0.6 and 0.01 pb at a CL of 95% for LQ_3 masses between 300 and 1500 GeV, assuming a branching fraction of $\beta = 1$. Third-generation scalar leptoquarks are excluded with masses below 900 GeV for $\beta = 1$.

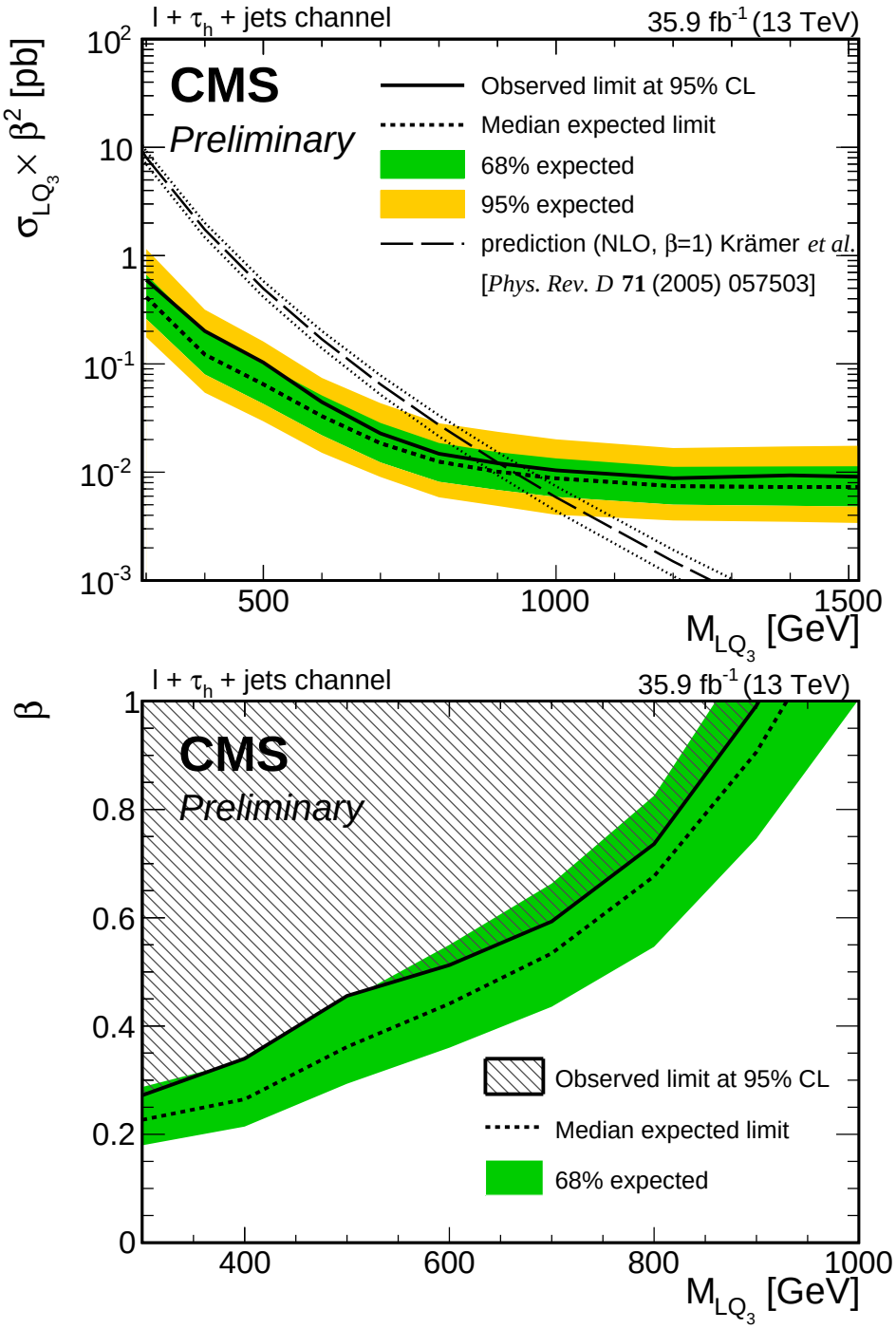

Figure 5: Upper limits at 95% confidence level on the cross section times branching fraction squared (top) and the leptoquark mass as a function of the branching ratio (bottom) on the pair production of scalar leptoquarks decaying to a top quark and a τ lepton. The results include all search categories in the ℓ+τ_h+jets channels. In the top plot, the theory curve corresponds to the NLO cross section with uncertainties from PDF and scale variations [34].

This result represents the most stringent limits to date on third-generation leptoquarks coupled to τ leptons and top quarks, constraining for the first time models explaining flavor anomalies in the B sector through contributions from scalar leptoquarks.

References

[1] W. Buchmüller, R. Rückl, and D. Wyler, "Leptoquarks in lepton-quark collisions", *Phys. Lett. B* **191** (1987) 442, doi:10.1016/0370-2693(87)90637-X. [Erratum: doi:10.1016/S0370-2693(99)00014-3].

[2] J. C. Pati and A. Salam, "Lepton number as the fourth "color"", *Phys. Rev. D* **10** (1974) 275, doi:10.1103/PhysRevD.10.275. [Erratum: doi:10.1103/PhysRevD.11.703.2].

[3] H. Georgi and S. L. Glashow, "Unity of all elementary particle forces", *Phys. Rev. Lett.* **32** (1974) 438, doi:10.1103/PhysRevLett.32.438.

[4] H. Fritzsch and P. Minkowski, "Unified interactions of leptons and hadrons", *Ann. Phys.* **93** (1975) 193, doi:10.1016/0003-4916(75)90211-0.

[5] E. Farhi and L. Susskind, "Technicolor", *Phys. Rept.* **74** (1981) 277, doi:10.1016/0370-1573(81)90173-3.

[6] K. D. Lane and M. V. Ramana, "Walking technicolor signatures at hadron colliders", *Phys. Rev. D* **44** (1991) 2678, doi:10.1103/PhysRevD.44.2678.

[7] B. Schrempp and F. Schrempp, "Light leptoquarks", *Phys. Lett. B* **153** (1985) 101, doi:10.1016/0370-2693(85)91450-9.

[8] B. Gripaios, "Composite leptoquarks at the LHC", *JHEP* **02** (2010) 045, doi:10.1007/JHEP02(2010)045, arXiv:0910.1789.

[9] BaBar Collaboration, "Evidence for an excess of $\bar{B} \to D^{(*)}\tau^-\bar{\nu}_\tau$ decays", *Phys. Rev. Lett.* **109** (2012) 101802, doi:10.1103/PhysRevLett.109.101802, arXiv:1205.5442.

[10] BaBar Collaboration, "Measurement of an excess of $\bar{B} \to D^{(*)}\tau^-\bar{\nu}_\tau$ decays and implications for charged Higgs bosons", *Phys. Rev. D* **88** (2013) 072012, doi:10.1103/PhysRevD.88.072012, arXiv:1303.0571.

[11] Belle Collaboration, "Observation of $B^0 \to D^{*-}\tau^+\nu_\tau$ decay at Belle", *Phys. Rev. Lett.* **99** (2007) 191807, doi:10.1103/PhysRevLett.99.191807, arXiv:0706.4429.

[12] Belle Collaboration, "Observation of $B^+ \to \bar{D}^{*0}\tau^+\nu_\tau$ and Evidence for $B^+ \to \bar{D}^0\tau^+\nu_\tau$ at Belle", *Phys. Rev. D* **82** (2010) 072005, doi:10.1103/PhysRevD.82.072005, arXiv:1005.2302.

[13] Belle Collaboration, "Measurement of the branching ratio of $\bar{B} \to D^{(*)}\tau^-\bar{\nu}_\tau$ relative to $\bar{B} \to D^{(*)}\ell^-\bar{\nu}_\ell$ decays with hadronic tagging at Belle", *Phys. Rev. D* **92** (2015) 072014, doi:10.1103/PhysRevD.92.072014, arXiv:1507.03233.

[14] LHCb Collaboration, "Measurement of the ratio of branching fractions $\mathcal{B}(\bar{B}^0 \to D^{*+}\tau^-\bar{\nu}_\tau)/\mathcal{B}(\bar{B}^0 \to D^{*+}\mu^-\bar{\nu}_\mu)$", *Phys. Rev. Lett.* **115** (2015) 111803, doi:10.1103/PhysRevLett.115.159901, 10.1103/PhysRevLett.115.111803, arXiv:1506.08614. [Erratum: Phys. Rev. Lett. 115, 159901 (2015)].

[15] B. Dumont, K. Nishiwaki, and R. Watanabe, "LHC constraints and prospects for S_1 scalar leptoquark explaining the $\bar{B} \to D^{(*)}\tau\bar{\nu}$ anomaly", *Phys. Rev.* **D94** (2016) 034001, doi:10.1103/PhysRevD.94.034001, arXiv:1603.05248.

[16] M. Tanaka and R. Watanabe, "New physics in the weak interaction of $\bar{B} \to D^{(*)}\tau\bar{\nu}$", *Phys. Rev. D* **87** (2013) 034028, doi:10.1103/PhysRevD.87.034028, arXiv:1212.1878.

[17] Y. Sakaki, M. Tanaka, A. Tayduganov, and R. Watanabe, "Testing leptoquark models in $\bar{B} \to D^{(*)}\tau\bar{\nu}$", *Phys. Rev. D* **88** (2013) 094012, doi:10.1103/PhysRevD.88.094012, arXiv:1309.0301.

[18] I. Doršner, S. Fajfer, N. Košnik, and I. Nišandžić, "Minimally flavored colored scalar in $\bar{B} \to D^{(*)}\tau\bar{\nu}$ and the mass matrices constraints", *JHEP* **11** (2013) 084, doi:10.1007/JHEP11(2013)084, arXiv:1306.6493.

[19] B. Gripaios, M. Nardecchia, and S. A. Renner, "Composite leptoquarks and anomalies in B-meson decays", *JHEP* **05** (2015) 006, doi:10.1007/JHEP05(2015)006, arXiv:1412.1791.

[20] S. Chakdar, T. Li, S. Nandi, and S. K. Rai, "Unity of elementary particles and forces for the third family", *Phys. Lett. B* **718** (2012) 121, doi:10.1016/j.physletb.2012.10.021, arXiv:1206.0409.

[21] S. Chakdar, T. Li, S. Nandi, and S. K. Rai, "Top SU(5) Models: Baryon and lepton number violating resonances at the LHC", *Phys. Rev. D* **87** (2013), no. 9, 096002, doi:10.1103/PhysRevD.87.096002, arXiv:1302.6942.

[22] CMS Collaboration, "Search for Third-Generation Scalar Leptoquarks in the tτ Channel in Proton-Proton Collisions at $\sqrt{s}$ = 8 TeV", *JHEP* **07** (2015) 042, doi:10.1007/JHEP11(2016)056, 10.1007/JHEP07(2015)042, arXiv:1503.09049. [Erratum: JHEP11,056(2016)].

[23] D0 Collaboration, "Search for third-generation leptoquarks in $p\bar{p}$ collisions at $\sqrt{s} = 1.96$ TeV", *Phys. Rev. Lett.* **99** (2007) 061801, doi:10.1103/PhysRevLett.99.061801, arXiv:0705.0812.

[24] CDF Collaboration, "Search for third generation vector leptoquarks in $p\bar{p}$ collisions at $\sqrt{s} = 1.96$ TeV", *Phys. Rev. D* **77** (2008) 091105, doi:10.1103/PhysRevD.77.091105, arXiv:0706.2832.

[25] ATLAS Collaboration, "Search for third generation scalar leptoquarks in pp collisions at $\sqrt{s} = 7$ TeV with the ATLAS detector", *JHEP* **06** (2013) 033, doi:10.1007/JHEP06(2013)033, arXiv:1303.0526.

[26] CMS Collaboration, "Search for third-generation leptoquarks and scalar bottom quarks in pp collisions at $\sqrt{s} = 7$ TeV", *JHEP* **12** (2012) 055, doi:10.1007/JHEP12(2012)055, arXiv:1210.5627.

[27] CMS Collaboration, "Search for pair production of third-generation scalar leptoquarks and top squarks in proton-proton collisions at $\sqrt{s}$ = 8 TeV", *Phys. Lett. B* **739** (2014) 229, doi:10.1016/j.physletb.2014.10.063, arXiv:1408.0806.

[28] CMS Collaboration, "Searches for third-generation squark production in fully hadronic final states in proton-proton collisions at $\sqrt{s} = 8$ TeV", *JHEP* **06** (2015) 116, doi:10.1007/JHEP06(2015)116, arXiv:1503.08037.

[29] ATLAS Collaboration, "Searches for scalar leptoquarks in pp collisions at $\sqrt{s} = 8$ TeV with the ATLAS detector", *Eur. Phys. J. C* **76** (2016) 5, doi:10.1140/epjc/s10052-015-3823-9, arXiv:1508.04735.

[30] CMS Collaboration, "Search for heavy neutrinos or third-generation leptoquarks in final states with two hadronically decaying τ leptons and two jets in proton-proton collisions at $\sqrt{s} = 13$ TeV", *JHEP* **03** (2017) 077, doi:10.1007/JHEP03(2017)077, arXiv:1612.01190.

[31] CMS Collaboration, "Search for third-generation scalar leptoquarks and heavy right-handed neutrinos in final states with two tau leptons and two jets in proton-proton collisions at $\sqrt{s} = 13$ TeV", *JHEP* **07** (2017) 121, doi:10.1007/JHEP07(2017)121, arXiv:1703.03995.

[32] G. R. Farrar and P. Fayet, "Phenomenology of the Production, Decay, and Detection of New Hadronic States Associated with Supersymmetry", *Phys. Lett.* **76B** (1978) 575–579, doi:10.1016/0370-2693(78)90858-4.

[33] R. Barbier et al., "R-parity violating supersymmetry", *Phys. Rept.* **420** (2005) 1–202, doi:10.1016/j.physrep.2005.08.006, arXiv:hep-ph/0406039.

[34] M. Krämer, T. Plehn, M. Spira, and P. M. Zerwas, "Pair production of scalar leptoquarks at the CERN LHC", *Phys. Rev. D* **71** (2005) 057503, doi:10.1103/PhysRevD.71.057503, arXiv:hep-ph/0411038.

[35] CMS Collaboration, "The CMS experiment at the CERN LHC", *JINST* **3** (2008) S08004, doi:10.1088/1748-0221/3/08/S08004.

[36] CMS Collaboration, "CMS luminosity measurements for the 2016 data taking period", *CMS Physics Analysis Summary* **CMS-PAS-LUM-17-001** (2017).

[37] T. Sjöstrand, S. Mrenna, and P. Z. Skands, "A Brief Introduction to PYTHIA 8.1", *Comput.Phys.Commun.* **178** (2008) 852–867, doi:10.1016/j.cpc.2008.01.036, arXiv:0710.3820.

[38] P. Nason, "A New method for combining NLO QCD with shower Monte Carlo algorithms", *JHEP* **11** (2004) 040, doi:10.1088/1126-6708/2004/11/040, arXiv:hep-ph/0409146.

[39] S. Frixione, P. Nason, and C. Oleari, "Matching NLO QCD computations with Parton Shower simulations: the POWHEG method", *JHEP* **11** (2007) 070, doi:10.1088/1126-6708/2007/11/070, arXiv:0709.2092.

[40] S. Alioli, P. Nason, C. Oleari, and E. Re, "A general framework for implementing NLO calculations in shower Monte Carlo programs: the POWHEG BOX", *JHEP* **06** (2010) 043, doi:10.1007/JHEP06(2010)043, arXiv:1002.2581.

[41] S. Frixione, P. Nason, and G. Ridolfi, "A positive-weight next-to-leading-order Monte Carlo for heavy flavour hadroproduction", *JHEP* **09** (2007) 126, doi:10.1088/1126-6708/2007/09/126, arXiv:0707.3088.

[42] S. Alioli, P. Nason, C. Oleari, and E. Re, "NLO single-top production matched with shower in POWHEG: s- and t-channel contributions", *JHEP* **09** (2009) 111, doi:10.1007/JHEP02(2010)011, 10.1088/1126-6708/2009/09/111, arXiv:0907.4076. [Erratum: JHEP02,011(2010)].

[43] E. Re, "Single-top Wt-channel production matched with parton showers using the POWHEG method", *Eur. Phys. J. C* **71** (2011) 1547, doi:10.1140/epjc/s10052-011-1547-z, arXiv:1009.2450.

[44] J. Alwall et al., "The automated computation of tree-level and next-to-leading order differential cross sections, and their matching to parton shower simulations", *JHEP* **07** (2014) 079, doi:10.1007/JHEP07(2014)079, arXiv:1405.0301.

[45] R. Frederix and S. Frixione, "Merging meets matching in MC@NLO", *JHEP* **12** (2012) 061, doi:10.1007/JHEP12(2012)061, arXiv:1209.6215.

[46] M. L. Mangano, M. Moretti, F. Piccinini, and M. Treccani, "Matching Matrix Elements and Shower Evolution for Top-Quark Production in Hadronic Collisions", *JHEP* **01** (2007) 013, doi:10.1088/1126-6708/2007/01/013, arXiv:hep-ph/0611129.

[47] CMS Collaboration, "Event generator tunes obtained from underlying event and multiparton scattering measurements", *Eur. Phys. J.* **C76** (2016), no. 3, 155, doi:10.1140/epjc/s10052-016-3988-x, arXiv:1512.00815.

[48] P. Skands, S. Carrazza, and J. Rojo, "Tuning PYTHIA 8.1: the Monash 2013 Tune", *Eur. Phys. J. C* **74** (2014) 3024, doi:10.1140/epjc/s10052-014-3024-y, arXiv:1404.5630.

[49] NNPDF Collaboration, "Parton distributions for the LHC Run II", *JHEP* **04** (2015) 040, doi:10.1007/JHEP04(2015)040, arXiv:1410.8849.

[50] CMS Collaboration, "Particle-flow reconstruction and global event description with the CMS detector", *JINST* **12** (2017), no. 10, P10003, doi:10.1088/1748-0221/12/10/P10003, arXiv:1706.04965.

[51] CMS Collaboration, "Description and performance of track and primary-vertex reconstruction with the CMS tracker", *JINST* **9** (2014) P10009, doi:10.1088/1748-0221/9/10/P10009, arXiv:1405.6569.

[52] M. Cacciari, G. P. Salam, and G. Soyez, "The Anti-k_t jet clustering algorithm", *JHEP* **04** (2008) 063, doi:10.1088/1126-6708/2008/04/063, arXiv:0802.1189.

[53] M. Cacciari, G. P. Salam, and G. Soyez, "FastJet user manual", *Eur. Phys. J. C* **72** (2012) 1896, doi:10.1140/epjc/s10052-012-1896-2, arXiv:1111.6097.

[54] CMS Collaboration, "Performance of CMS muon reconstruction in pp collision events at $\sqrt{s} = 7$ TeV", *JINST* **7** (2012) P10002, doi:10.1088/1748-0221/7/10/P10002, arXiv:1206.4071.

[55] CMS Collaboration, "Performance of electron reconstruction and selection with the CMS Detector in proton-proton collisions at $\sqrt{s} = 8$ TeV", *JINST* **10** (2015) P06005, doi:10.1088/1748-0221/10/06/P06005, arXiv:1502.02701.

[56] M. Cacciari, G. P. Salam, and G. Soyez, "The catchment area of jets", *JHEP* **04** (2008) 005, doi:10.1088/1126-6708/2008/04/005, arXiv:0802.1188.

[57] CMS Collaboration, "Determination of jet energy calibration and transverse momentum resolution in CMS", *JINST* **6** (2011) P11002, doi:10.1088/1748-0221/6/11/P11002, arXiv:1107.4277.

[58] CMS Collaboration, "Jet energy scale and resolution in the CMS experiment in pp collisions at 8 TeV", *JINST* **12** (2017), no. 02, P02014, doi:10.1088/1748-0221/12/02/P02014, arXiv:1607.03663.

[59] CMS Collaboration, "Identification of b-quark jets with the CMS experiment", *JINST* **8** (2013) P04013, doi:10.1088/1748-0221/8/04/P04013, arXiv:1211.4462.

[60] CMS Collaboration, "Identification of b quark jets at the CMS experiment in the LHC Run 2", *CMS Physics Analysis Summary* **CMS-PAS-BTV-15-001** (2016).

[61] CMS Collaboration, "Performance of tau-lepton reconstruction and identification in CMS", *JINST* **7** (2012) P01001, doi:10.1088/1748-0221/7/01/P01001, arXiv:1109.6034.

[62] CMS Collaboration, "Performance of reconstruction and identification of tau leptons in their decays to hadrons and tau neutrino in LHC Run-2", *CMS Physics Analysis Summary* **CMS-PAS-TAU-16-002** (2017).

[63] CMS Collaboration, "Performance of the CMS missing transverse momentum reconstruction in pp data at $\sqrt{s}$ = 8 TeV", *JINST* **10** (2015), no. 02, P02006, doi:10.1088/1748-0221/10/02/P02006, arXiv:1411.0511.

[64] CMS Collaboration, "Measurement of the $t\bar{t}$ production cross section using events in the eμ final state in pp collisions at $\sqrt{s} = 13$ TeV", *Eur. Phys. J.* **C77** (2017) 172, doi:10.1140/epjc/s10052-017-4718-8, arXiv:1611.04040.

[65] N. Kidonakis, "NNLL threshold resummation for top-pair and single-top production", *Phys. Part. Nucl.* **45** (2014) 714, doi:10.1134/S1063779614040091, arXiv:1210.7813.

[66] CMS Collaboration, "Observation of the associated production of a single top quark and a W boson in pp collisions at sqrt(s) = 8 TeV", *Phys. Rev. Lett.* **112** (2014) 231802, doi:10.1103/PhysRevLett.112.231802, arXiv:1401.2942.

[67] CMS Collaboration, "Cross section measurement of t-channel single top quark production in pp collisions at $\sqrt{s} = 13$ TeV", *Submitted to: Phys. Lett. B* (2016) arXiv:1610.00678.

[68] CMS Collaboration, "Measurement of inclusive W and Z boson production cross sections in pp collisions at $\sqrt{s}$ = 8 TeV", *Phys. Rev. Lett.* **112** (2014) 191802, doi:10.1103/PhysRevLett.112.191802, arXiv:1402.0923.

[69] J. M. Campbell, R. K. Ellis, and C. Williams, "Vector boson pair production at the LHC", *JHEP* **07** (2011) 018, doi:10.1007/JHEP07(2011)018, arXiv:1105.0020.

[70] T. Gehrmann et al., "W^+W^- Production at Hadron Colliders in Next-to-Next-to-Leading-Order QCD", *Phys. Rev. Lett.* **113** (2014) 212001, doi:10.1103/PhysRevLett.113.212001, arXiv:1408.5243.

[71] CMS Collaboration, "Measurement of the inelastic proton-proton cross section at $\sqrt{s} = 7$ TeV", *Phys. Lett.* **B722** (2013) 5–27, doi:10.1016/j.physletb.2013.03.024, arXiv:1210.6718.

[72] J. Butterworth et al., "PDF4LHC recommendations for LHC Run II", *J. Phys.* **G43** (2016) 023001, doi:10.1088/0954-3899/43/2/023001, arXiv:1510.03865.

[73] J. Ott, “theta - a framework for template-based modeling and inference”, http://www.theta-framework.org.